Surface relaxation phenomena at electrified interfaces: Revealing adsorbate, potential, and solvent effects by combined x-ray diffraction, STM and DFT studies

Martino Saracino,[1,2] Peter Broekmann,[3,4,*] Knud Gentz,[3] Moritz Becker,[1] Hubert Keller,[2] Florian Janetzko,[3] Thomas Bredow,[3] Klaus Wandelt,[3] and Helmut Dosch[1,2]

[1]*Max-Planck-Institut für Metallforschung, Heisenbergstrasse 3, 70569 Stuttgart, Germany*

[2]*Institut für Theoretische und Angewandte Physik, Universität Stuttgart, Pfaffenwaldring 57, 70569 Stuttgart, Germany*

[3]*Institut für Physikalische und Theoretische Chemie, Universität Bonn, Wegelerstrasse 12, 53115 Bonn, Germany*

[4]*Departement für Chemie und Biochemie, Universität Bern, Freiestrasse 3, 3012 Bern, Switzerland*

(Received 16 December 2008; revised manuscript received 28 January 2009; published 31 March 2009)

Surface relaxation phenomena have been studied in an electrochemical environment using halide modified Cu(100) electrodes as model systems to unravel the impact of the chemical nature of the adsorbed halide, the applied potential, and the presence of solvent species on the surface interlayer spacings. Both, *in situ* STM and *in situ* x-ray scattering data point to *lateral* structures of the adsorbed halides on Cu(100) which are identical for both chloride and bromide. Under saturation conditions both halides form a $p(1\times1)$ adlayer on Cu(100) with reference to a conventional choice of the substrate fcc unit cell. The *in situ* x-ray scattering data clearly indicate that the copper-halide and the copper-copper interlayer spacings are much more affected by potential changes when bromide is adsorbed on the copper surface and are less affected when chloride is present. This difference in the potential dependence of both halides can be attributed to the larger polarizability of the bromide anion that is almost discharged on the copper surface at the highest applied potentials, while chloride remains largely ionic in the adsorbed state even at the highest applied potential. At the lowest applied potential of $E_{\mathrm{work}}=-150$ mV [vs reversible hydrogen electrode (RHE)] the Br-Cu and the topmost Cu-Cu layer distances are expanded by 0.150 and 0.058 Å, respectively, with reference to their bulk analogs CuBr and Cu. These spacings continuously contract by up to 0.075 and 0.038 Å when the electrode potential is increased to $E_{\mathrm{work}}=+50$ mV (RHE). Intriguingly, the second Cu layer experiences a potential-dependent buckling due to a different second-shell coordination of Cu by bromide while deeper Cu layers retain the bulk spacing at all potentials. Changes in the halide-copper and the copper-copper interlayer spacings are strongly correlated. An understanding of the *in situ* x-ray results is achieved by periodic quantum-chemical calculations at density-functional level that allow a modeling of the interfacial structure under consideration of *potential* and additional *solvation effects*. The latter originate from interaction of water molecules and counterions in the *outer Helmholtz layer* with the specifically adsorbed halides in the *inner Helmholtz layer*.

DOI: 10.1103/PhysRevB.79.115448 PACS number(s): 68.08.−p, 61.05.cf, 68.37.Ef

I. INTRODUCTION

The microscopic understanding of charge-transfer reaction kinetics in electrochemical environments requires detailed knowledge of the atomic-scale structure of the respective solid/liquid interface. However, such a fundamental understanding is often lacking even for technologically and economically highly relevant processes. One of the most prominent examples hereof is the state-of-the-art on-chip wiring of transistors on Si wafers which is today based on an electrochemical copper deposition, also known as *(dual) damascene process*.[1–5] In most of today's logic devices copper has replaced aluminum as the preferred wiring material. In order to build up three-dimensional (3D) wiring architectures copper has to grow within the "vias" and "trenches" of the patterned substrate in a superconformal mode ("superfilling"). This requires a so-called bottom-up filling of these features with copper material, a process which depends sensitively on the composition of the plating baths.

Halides which are commonly added in trace amounts to the plating bath are known as crucial additives. While chloride acts as an accelerator, at least in the absence of other additives, bromide suppresses the copper deposition.[6,7] The role of adsorbed halides in the copper electrodeposition process is diverse. When present in the plating baths halides are specifically adsorbed on the copper surface during copper deposition. Therefore, much attention has been paid in the past to the characterization of the lateral ordering and the potential-dependent phase behavior of halides on copper surfaces, particularly focusing here on idealized single crystalline copper surfaces that allow the use of advanced structure sensitive surface science tools such as the *in situ* scanning tunnel microscope (STM).[8–14] The lateral mobility of cuprous and cupric species can be affected by the presence of halides.[15] Adsorbed halide layers can further act as binding partners to other additives, e.g., so-called levelers which are typically monomeric, oligomeric, or polymeric N-containing (poly)-cations which are assumed to interact electrostatically with the halide modified copper surface.[16–19] At first sight chloride and bromide behave quite similar when adsorbed on the copper surface. For instance, under saturation conditions both halides form a well-ordered adsorbate phase on Cu(100) that has often been described in literature by a Cu(100)-$c(2\times2)$-X or as a $(\sqrt{2}\times\sqrt{2})R45°$-$X$ (X=Cl, Br) superstructure,[8–14,20] which is identical with our simple $p(1\times1)$ notation. The unconventional choice of a unit cell for the Cu substrate is only based on its asymmetric unit and leads to a Cu(100)-$c(2\times2)$-X or to a $(\sqrt{2}\times\sqrt{2})R45°$ descrip-

tion of the superstructure cell after halide adsorption. However, the conventional choice or the Cu substrate based on an fcc lattice leads to a simpler $p(1\times1)$ overlayer geometry description [see Fig. 2(e)]. This notation will be used throughout the paper.

While the lateral structure of the above-mentioned halides is well documented in literature much less is known about the structural impact of these halides on the underlying copper substrate in terms of surface relaxation effects.[21] Weakening or strengthening of the copper-copper bond by the presence of adsorbed halides is assumed to have a significant impact on important phenomena such as the "electrochemical (self-)annealing."[15]

It is actually the potential applied to the Cu(100) surface in an electrochemical environment which can be used to fine tune the interlayer separations while keeping the lateral structure of the interface unchanged. Crucial for the magnitude of these potential-dependent interlayer expansions/contractions (*potential effects*) is the chemical nature of the halide adsorbed on the copper surface. What also needs to be considered when working with electrochemical systems is the presence of solvent molecules and counterions in the "outer" and "diffuse" Helmholtz layers in vicinity of the specifically adsorbed halides (solvation effects). These additional binding partners of the halides on the electrolyte side are expected to also have an impact on the copper-halide and copper-copper bonds inside the electrode.

Since all these structural effects are beyond the pure surface imaging by STM we have to apply more sophisticated structure sensitive techniques. In the present contribution we report the full 3D structure of the copper/electrolyte interface in the presence of halide monolayers which has been obtained by *in situ* x-ray diffraction under realistic electrochemical conditions (hanging droplet technique). In this way we unraveled potential-dependent surface relaxation phenomena in the presence of bromide monolayers and were able to compare them to earlier results for chloride-covered Cu(100) surfaces[21] and to data obtained from previous ultrahigh vacuum (UHV) work. It is the comparison of the UHV work with our data obtained in an electrochemical environment that unravels the specific impact of an additional electrolyte phase (in particular the outer and diffuse Helmholtz layers) on the surface relaxation effects.

A promising approach toward basic understanding of all the structural phenomena observed in the *in situ* x-ray diffraction experiment relies on theoretical models that consider indeed both potential and solvation effects. During the past years, quantum-chemical techniques, mainly, based on density-functional theory (DFT), have been established as reliable tools for the investigation of complex bulk and surface phenomena at atomic scale.[22] They can also provide new insights in the bonding mechanisms of molecules at surfaces. However, most theoretical studies have focused on the adsorption under UHV conditions.[23–27] The inclusion of solvent effects within the Helmholtz layer above the electrode surface and the electrochemical potential appears to be a new challenge for theoretical models.[28]

Recently, Marx *et al.*[29] studied the peptide synthesis at pyrite surfaces in aqueous media with DFT molecular-dynamics techniques. A common approach to simulate the potential is to apply an external field, mainly, in combination with finite cluster models of the surface.[30] This approach has the disadvantage that the potential varies also inside the metal. A physically more meaningful approach has been developed by Neurock and co-workers[31,32] in recent DFT studies of adsorption processes on metal surfaces. The potential was modeled by adding a fractional charge to a periodic supercell model of the system. The extra charges were compensated by a uniform background charge of opposite sign. The half-cell potential was directly calculated by the Fermi energy of the metal surface corrected by the potential difference at the surface and in the solvent volume.

II. EXPERIMENTAL METHOD

The scanning tunneling microscopy (STM) experiments presented in this paper were carried out using a specifically designed set-up[33] that has been described elsewhere.[34]

The x-ray scattering experiments reported here have been performed under potential control in an electrochemical cell and with a synchrotron beam energy of 18 keV provided by beamline ID32 at the European Synchrotron Radiation Facility in Grenoble.

The Cu crystal was 5 mm in diameter and polished to within 0.2° of the crystallographic (100) plane. The bulk mosaic was 0.07° at the (1,0,1) reflection. The experimental sample environment and preparation was comparable to that of the STM experiments in Refs. 34–36. The Cu crystal was electropolished in 50% H_3PO_4 to remove the surface oxide and subsequently treated in a 10 mM HCl solution. Under these conditions a monolayer of chloride ions adsorbs at the Cu(100) surface even under open circuit conditions and prevents reoxidation. Such a treatment in an acidic and chloride containing electrolyte further facilitates the so-called self-annealing of defects originated from the initial electrochemical polishing preparation step. The crystal was then mounted as working electrode in the electrochemical cell that contained a 5 mM H_2SO_4/10 mM KCl solution. The electrochemical cell design is shown in Fig. 1(a). A representative cyclic voltammogram obtained in the hanging droplet configuration in the *in situ* x-ray scattering cell is presented in Fig. 1(b). It is consistent with electrochemical measurements carried out in standard electrochemical cells or *in situ* STM cells. The arrows k_i and k_f indicate the incoming and scattered x-ray wave vector, respectively. Electrochemical reactions take place at the solid-liquid interface formed by a hanging droplet that covers the whole Cu(100) surface. The counter and reference electrode are placed in a capillary about 5–15 mm above the sample surface. Potential control of the sample is achieved through a potentiostat. All potentials were measured with reference to an Ag/AgBr electrode. For the sake of convenience, all potentials given in the paper are referred to the reversible hydrogen electrode (RHE). Sample, electrolyte and all electrical feedthroughs are separated from air by a 0.8 μm Kapton foil. The inside of the Kapton foil cylinder is flushed by high-purity N_2 gas.

Charging effects of the Cu substrate were studied by changing its potential within the stability range of the adsorbed $p(1\times1)$ Br layer, ranging from $E_{work}=-150$ mV to

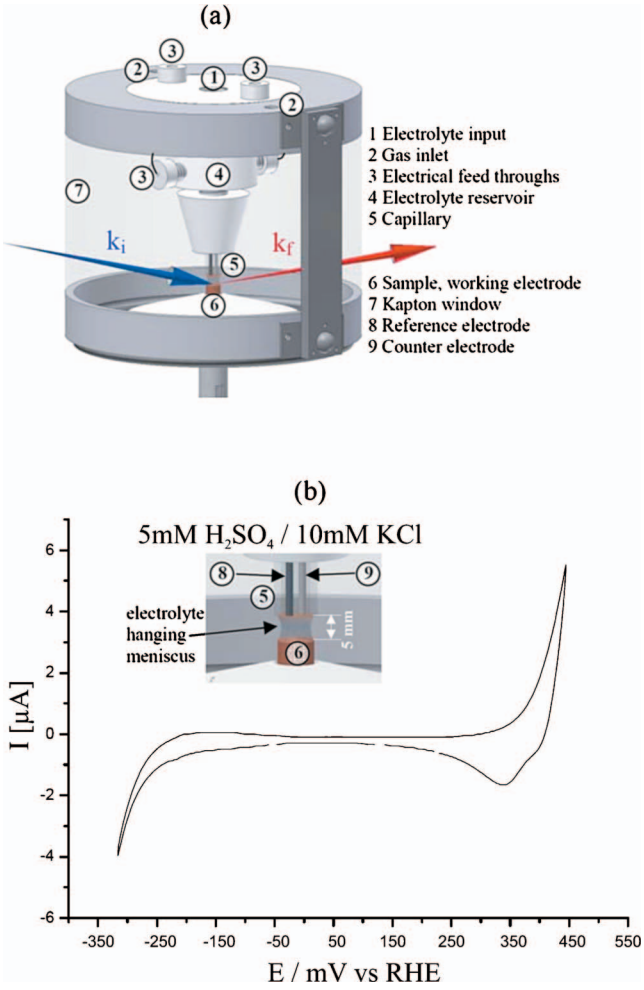

FIG. 1. (Color) (a) Sketch of electrochemical cell and (b) cyclic voltammogram of Cu(100) in 5 mM H_2SO_4/10 mM KCl as an example of electrochemical control over the sample, sweep rate: $dE/dt=10$ mV/s

$E_{work}=+50$ mV. For $E_{work}=+50$ mV, $E_{work}=-50$ mV, and $E_{work}=-150$ mV we measured the $(2,0,L)$ and $(2,2,L)$ crystal truncation rods (CTRs) (Ref. 37) and $(1,0,L)$ adlayer rod of Br on Cu(100)-$p(1\times1)$ up to a maximum normal momentum transfer of $Q_z=6.3$ Å^{-1}, which is equivalent to 3.6 reciprocal lattice units. All results are presented with reference to the crystallographic bulk notation of copper with a cubic face-centered unit cell and a lattice constant of $a_{Cu}=3.61$ Å at room temperature.

The x-ray diffraction analysis for each potential is based on the measurement of a total of 90–99 integrated out-of-plane intensities in z-axis geometry and at room temperature by rotating the sample around its surface normal and subtracting the diffuse background signal. The background was mainly caused by the electrolyte and by the Kapton foil that was used to seal the electrochemical cell from air. In order to correctly determine the strong background for data correction we made sufficiently expanded transverse scans for all measured reflections. The error of the diffraction intensities was estimated from the measured reproducibility of symmetry equivalent reflections and produced an internal R value of 10% based on $|F|^2$ for all reflections. All data were corrected for polarization, Lorentz factor, active sample area, and the resolution function of the instrument.

III. RESULTS AND DISCUSSION

A. STM results

For comparison, Fig. 2 displays the surface morphology and the atomic structure of the Cu(100) electrode in the presence of specifically adsorbed chloride (in the following abbreviated as Cl) and bromide (in the following abbreviated as Br) anions at potentials within the double layer regime. Both halide anions form the same saturation $p(1\times1)$ adlayer on Cu(100). Not only is the atomic-scale structure of the electrode surface affected by the adsorption of these halide anions but also the entire surface morphology, provided an adequate surface mobility has been induced at high electrode potentials close to the onset of the Cu dissolution reaction.[9–12,20] Halide-stabilized substrate steps are aligned parallel to the ⟨010⟩ directions which coincide with the close-packed halide rows. Furthermore, these ⟨010⟩ steps reveal an extremely low kink density after applying an "electrochemical annealing" procedure. These "morphological effects" result from tremendous changes in the step and kink energies induced by halide anion adlayers.

B. X-Ray diffraction analysis and discussion

The analysis of the $(2,0,L)$ and the $(2,2,L)$ CTRs together with the $(1,0,L)$ adlayer rod [see Figs. 3(a)–3(c)] confirms the presence of a $p(1\times1)$-Br adlayer on Cu(100) for substrate potentials of $E_{work}=+50$ mV, $E_{work}=-50$ mV, and $E_{work}=-150$ mV. The presence of only adlayer diffraction along the $(1,0,L)$ rod is due to the reflection conditions of the Cu substrate which shows no intensity at this position in reciprocal space. The primitive two-dimensional (2D) lattice of the overlayer has, however, no such restrictions.

The geometry of the bromide-covered Cu(100) surface is shown in Fig. 4. The fit parameters of the $p(1\times1)$-Br structure model include adlayer and surface layer occupancies, interlayer spacings of the Br-Cu and top Cu-Cu layer, and their Debye-Waller factors (DWFs). Lateral positional parameters stay fixed during the refinement due to symmetry restrictions given by their special positions within the unit cell and by the plane group symmetry $p4mm$. It was not necessary to include a surface roughness model in the fit which would account for statistically distributed up and down steps. The electrochemical annealing process and the resulting atomically smooth surfaces lead to roughness parameters close to zero. Therefore we kept the roughness parameters constant during the refinement. Since Bragg reflections along the CTRs were also included in the data collection we were able to apply an absolute scaling of the model to the data which improved the overall reliability of the fitted details for data between Bragg peaks and for different surface preparations.

Tables I(a)–I(c) contains all fit results. Table I(d) contains the interlayer distances calculated from the fitted z components of the model shown in Fig. 4 and listed in Table I(a). All layer distances are given in relative values of the Cu

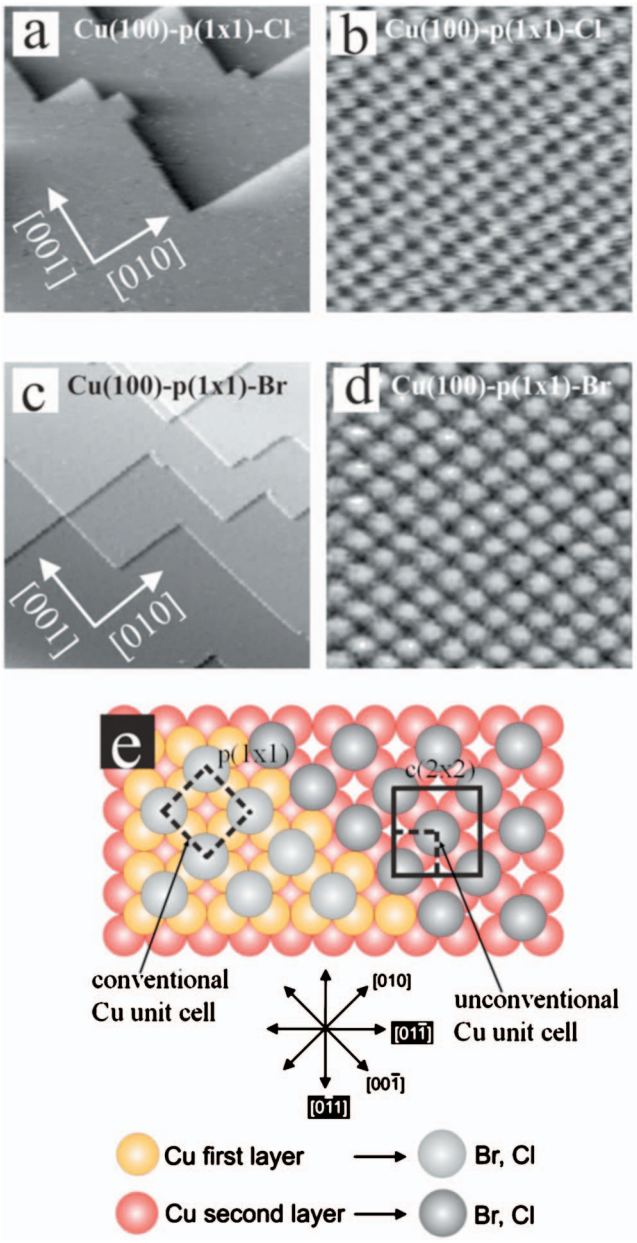

FIG. 2. (Color) (a) Morphology of the Cu(100) electrode in the presence of the $p(1\times1)$-Cl adlayer; 69×69 nm^2; $I_t=1$ nA, $U_b=25$ mV, and $E_{\text{work}}=+500$ mV vs RHE; (b) atomic structure of the $p(1\times1)$-Cl adlayer, 5.3×5.3 nm^2; $I_t=1$ nA, $U_b=25$ mV, and $E_{\text{work}}=+100$ mV vs RHE; (c) morphology of the Cu(100) electrode in the presence of the $p(1\times1)$-Br adlayer; 86×86 nm^2; $I_t=1$ nA, $U_b=5$ mV, and $E_{\text{work}}=+50$ mV vs RHE; (d) atomic structure of the $p(1\times1)$-Br adlayer, 3.2×3.2 nm^2; $I_t=1$ nA, $U_b=5$ mV, and $E_{\text{work}}=+50$ mV vs RHE; (e) Hard-sphere model of the $p(1\times1)$-halide adlayer with an additional unit-cell definition for a $c(2\times2)$ notation used in Refs. 8–14 and 20–24.

interlayer distance $a_{\text{Cu}}/2=1.807$ Å. Atomic positions are expressed in relative units of the lattice constant $a_{\text{Cu}}=3.614$ Å. Numbers in brackets indicate the error with respect to the last given digit of the fit parameter. Numbers without errors stayed fixed in the refinement. The agreement between model and data [Figs. 3(a)–3(c)] is expressed through a goodness of fit (GoF) with reference to a χ^2 criterion according to

$$\chi^2=\frac{1}{N-p}\frac{\sum_{hkl}||F_{hkl}^{\text{calc.}}|^2-|F_{hkl}^{\text{expt.}}|^2|}{\sigma_{hkl}},$$

with N as the quantity of measured structure factors, p as the quantity of fit parameters, and σ_{hkl} as error of $|F_{hkl}^{\text{expt.}}|^2$. The GoF in Table I(c) for each data set is close to 1 which means that within the range of the errors and for the given set of fit parameters there is barely any more significant information contained in the data which would change the model significantly. The solid lines in Figs. 3(a)–3(c) represent the best fit of our model and the dashed lines correspond to a model calculation of an ideal bulk-terminated Cu(100) substrate. The overall good agreement between data and model is obvious. However, there are systematic deviations for Q_z values below 0.5. These deviations are notable for the adlayer rod data in Fig. 3(c). They could not be eliminated by considering further fit parameters in the analysis such as deeper layer relaxations or additional ordering effects affecting solvent molecules or counterions in the outer or diffuse Helmholtz layer above the anion-modified electrode surface. In the present case deeper layers are set to bulk spacing by the fit and stay unchanged during the refinement. We assume that the data deviation at low Q_z values results from a very broad resolution function which is inherent to this kind of diffraction geometry. Finally, the significance, reliability, and large real-space resolution of the model is supported by the small errors of the positional fit parameters of maximal 0.0025 Å as can be deduced from Table I(a).

Our analysis leads to a decreasing Br-Cu adlayer spacing with increasing potential of the Cu electrode as shown in Fig. 5(a). At $E_{\text{work}}=-150$ mV we observe a $\Delta d_{\text{ad-1}}$ of 8.3(2)% meaning that the Br-Cu layer distance is 8.3(2)% larger than that of parallel Cu-Cu bulk layers. This value decreases to 5.6(2)% at $E_{\text{work}}=-50$ mV and finally to 4.2(1)% for $E_{\text{work}}=+50$ mV [Table I(a)]. As the adlayer distance decreases with potential the adlayer coverage θ increases from $\theta=0.766(2)$ to $\theta=0.899(2)$ and finally to $\theta=1.00(1)$ at $E_{\text{work}}=+50$ mV. This can be intuitively understood since the attractive electrostatic forces between the Cu electrode and the bromide ions are increased. Our model incorporates this fact by assuming that part of the Cu(100) surface is not covered by Br and has therefore no influence on its relaxation. In other words the structural parameters of the Br-covered surface do not depend on its coverage in our structural refinement. In summary, both results express a strengthening of the Br-Cu bond with increasing electrode potential. The resulting Br-Cu bond length is, however, expanded by 5.5% at $E_{\text{work}}=-150$ mV in comparison to its value of 2.46 Å in bulk CuBr.[38,39] This expansion diminishes with the compression of the Cu-adlayer spacing to 4.4% as the potential is increased to $E_{\text{work}}=+50$ mV. The remaining expansion of the Br-Cu distance can be understood by the fact that Br has four next-Cu neighbors in bulk and on Cu(100), however, in different coordination geometries. On Cu(100), Br resides on

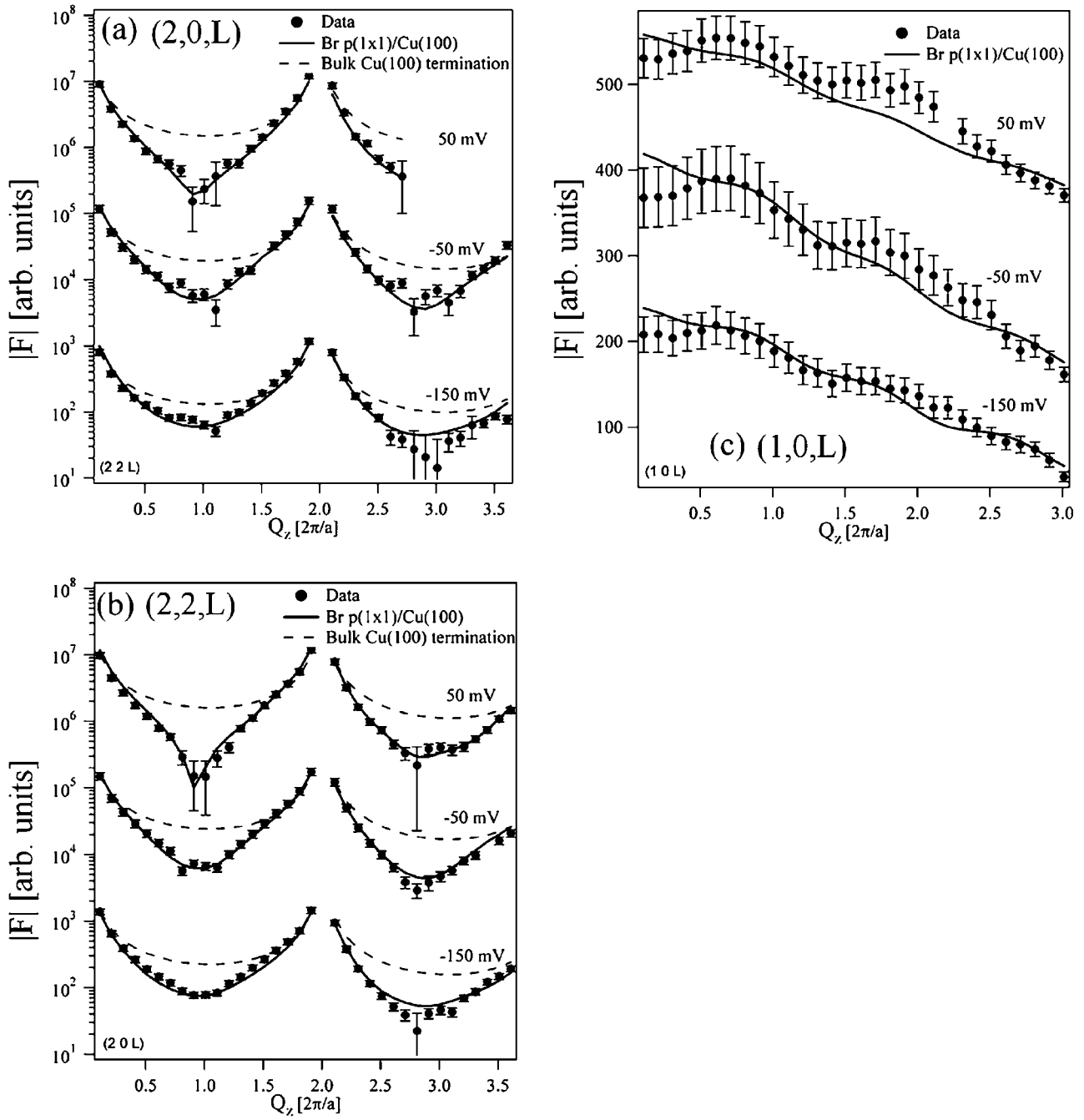

FIG. 3. Plot of the scattered amplitude $|F|$ along the (a) $(2,0,L)$ and (b) $(2,2,L)$ CTRs as function of momentum transfer perpendicular to the surface for Br on Cu(100). The filled circles represent the experimental values; the solid line represents the best fit based on the model shown in Fig. 4. The dashed line shows the calculated intensity based on an uncovered bulk terminated Cu(100) surface. (c) Plot of the intensity distribution along the $(1,0,L)$ adlayer rod.

fourfold hollow sites, in CuBr, Br is tetrahedrally coordinated by Cu.

The first Cu interlayer spacing shows an expansion at all applied potentials in Fig. 5(b). A maximum outward relaxation of $d_{1\text{-}\overline{2ab}}=3.2(1)\%$ is obtained at $E_{\text{work}}=-150$ mV. This relaxation drops to 2.7(1)% at $E_{\text{work}}=-50$ mV and 1.1(1)% for $E_{\text{work}}=+50$ mV (all numbers above are in rel. units of $a_{\text{Cu}}/2$).

It should be noted that such a decrease in copper-copper layer separation with increasing potentials is intuitively unexpected and surprising at least at first sight. A depletion of negative charge at the electrode surface with increasing potentials is expected to increase the copper-copper interlayer separation. Therefore, it is apparent that the observed effect is due to the presence of the bromide adlayer. Both, the potential-dependent halide-copper and the copper-copper interlayer spacings are strongly correlated with each other. An explanation for this behavior can be found in the particular charge state of bromide anions as they partially keep their negative charge upon adsorption from solution. This behav-

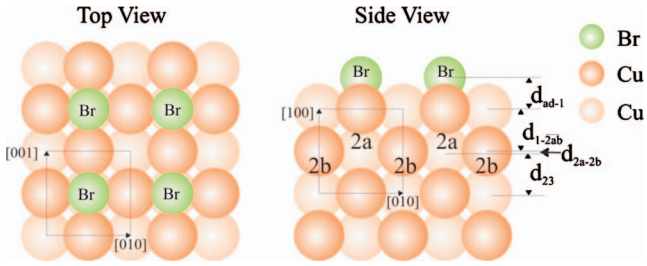

FIG. 4. (Color) Side and top views of the Br/Cu(100)-$p(1\times1)$ model. The side view indicates a series of layers and their labels as used in the text. The solid rectangle in both views represent the choice of unit cell with reference to the Cu(100) surface. The arrows define the crystallographic main directions.

ior is not uncommon for electrosorbed systems[40,41] and will be discussed in more detail below based on results of quantum-chemical simulations (Sec. III C).

A further interesting detail of the potential-dependent surface relaxation phenomena consists in a certain nonuniformity in the vertical movements of the copper atoms in the second layer of the copper substrate. Such nonuniformity can be understood in terms of "local" coordination effects of the adsorbed Br. Copper atoms in the second copper layer labeled 2*a* and 2*b* are not equivalent with respect to the covering bromide layer. Only every second copper atom is "coordinated" by Br (Fig. 4, side view). Typically the Br-coordinated copper atoms are more affected by the potential changes than the noncoordinated ones. The fit of the above model significantly improves by taking a "buckling" of the second Cu layer into account. The significance is justified by the reduction in the GoF by 10% on average and for all applied potentials. The nonuniformity in the coordination geometry leads to a difference in the local charge density above these Cu atoms. The z components of the respective Cu atoms differ accordingly. The buckling can be expressed by a

TABLE I. (a) Fitted atomic positions of Br/Cu(100)-$p(1\times1)$ as a function of the electrode potential, (b) Debye-Waller Factors, (c) coverage, roughness factor, goodness of fit for each experiment, amount of data, and (d) interlayer spacings in units of $a_{Cu}/2$.

(a)

Atom	x [a]	y [a]	z [a] (E_{Work}=−150 mV)	z [a] (E_{Work}=−50 mV)	z [a] (E_{Work}=50 mV)
Br	0.500	0.500	1.0552(7)	1.0413(9)	1.0319(3)
Cu	0.500	0.000	0.5138(3)	0.5132(3)	0.5110(2)
Cu	0.000	0.500	0.5138(3)	0.5132(3)	0.5110(2)
Cu	0.500	0.500	−0.0042(3)	−0.0016(2)	0.0046(2)
Cu	0.000	0.000	0.0001(2)	0.0007(3)	0.0062(3)

(b)

	Debye-Waller factor (Å^2)			
E_{Work} [mV RHE]	Adlayer	First Cu Layer	Second Cu Layer	Cu Bulk
50	3.97(3)	1.140(9)	0.76(1)	0.598
−50	5.44(4)	1.31(2)	0.35(2)	0.598
−150	5.23(3)	1.95(2)	0.97(1)	0.598

(c)

E_{Work} (mV RHE)	Coverage θ (ML)	Roughness β	Goodness of fit χ^2	Number of data points
50	1.00(1)	0.16	1.44	90
−50	0.899(2)	0.18	1.09	98
−150	0.766(2)	0.18	1.72	99

(d)

E_{Work} (mV RHE)	d_{ad-1} [$a/2$]	$d_{1-\overline{2ab}}$ [$a/2$]	d_{2a-2b} [$a/2$]	d_{2-3} [$a/2$]
50	1.042(1)	1.0112 (9)	0.003(1)	1.0054(5)
−50	1.056(2)	1.027(1)	0.005(1)	0.9996(5)
−150	1.083(2)	1.032(1)	0.009(1)	0.9979(5)

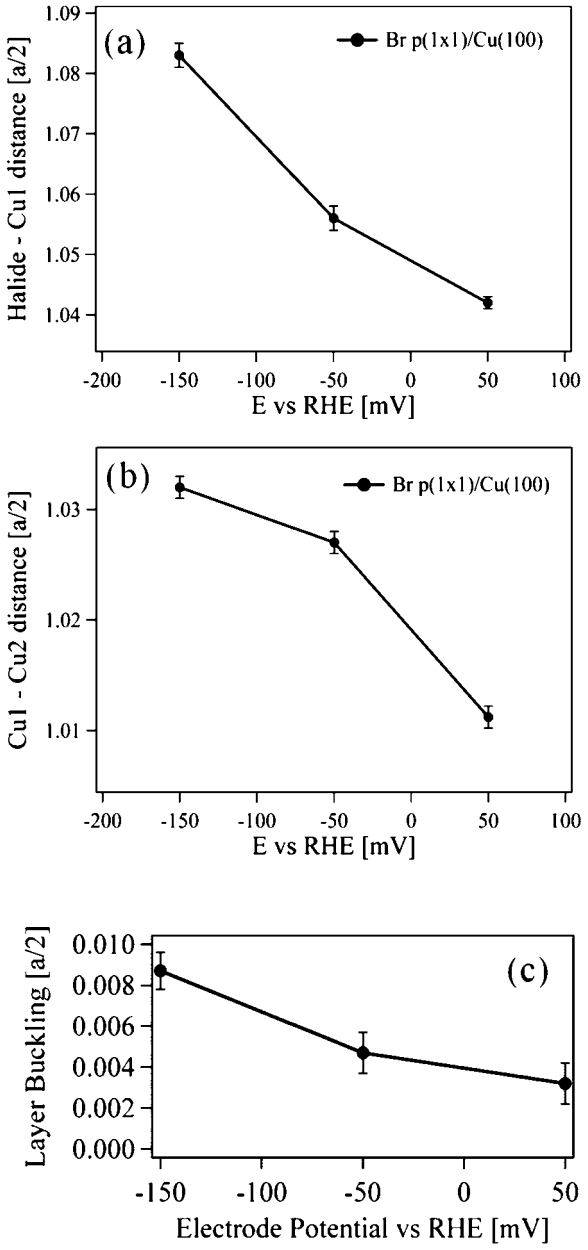

FIG. 5. (a) Plot of the potential-dependent Br-Cu distance, (b) plot of the potential-dependent topmost Cu-Cu distance, (c) plot of the potential-dependent layer buckling given in terms of the splitting of the relative z components of atoms $2a$ and $2b$ in Fig. 4.

separation of Cu_{2a} and Cu_{2b} in the z direction (Fig. 4). It follows the trend of the $d_{1\text{-}\overline{2ab}}$ relaxation and decreases with increasing potential from $d_{2a\text{-}2b}=0.009(1)$ at $E_{\text{work}}=-150$ mV to $d_{2a\text{-}2b}=0.003(1)$ at $E_{\text{work}}=+50$ mV [Fig. 5(c)]. The presence of a second layer buckling has also been observed in an angle-resolved ultraviolet photoemission spectroscopy (ARUPS) study of Cl/Cu(100) by Wang *et al.*[42] who found a buckling amplitude of $d_{2a\text{-}2b}=0.02(1)$.

The experimentally observed larger spacings between the topmost atomic layers point to weaker restoring forces among them and hence to increased Debye-Waller factors [Table I(b)]. The largest DWFs are found at the most negative potential of $E_{\text{work}}=-150$ mV. The layer formed by the

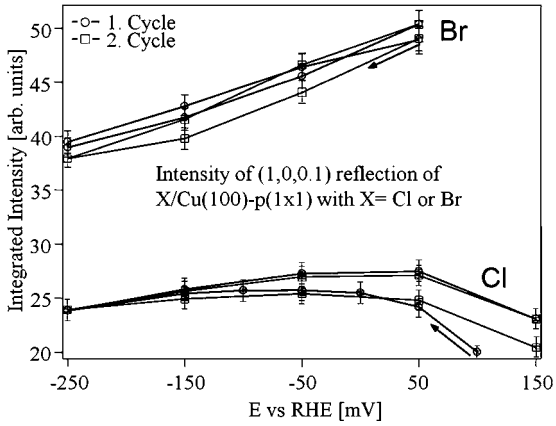

FIG. 6. Potential-dependent behavior of the surface-sensitive integrated intensities of the (1,0,0.1) reflection of Br/Cu(100). Data points corresponding to two full cycles within the potential range of $E_{\text{work}}=-250$ mV to $E_{\text{work}}=+150$ mV are presented.

atoms $2a$ and $2b$ (Fig. 4) shows an increase in its DWF to 0.97(1) Å^2 with reference to the Cu bulk value of 0.598 Å^2. The DWF of the topmost Cu layer roughly triples this value to 1.95(2) Å^2. The DWF of the Br atom is 5.23(3) Å^2. On average there is an increase in the DWF within the potential window from $E_{\text{work}}=+50$ mV to $E_{\text{work}}=-150$ mV and with reference to the Cu bulk value by a factor of 1.16(2) for the second Cu layer, by a factor of 2.45(3) for the top Cu layer, and a factor of 8.16(7) for Br.

Although both Br and Cl form a $p(1\times1)$ adlayer on Cu(100) there are pronounced differences in their potential-dependent behavior. Figure 6 shows the integrated intensity of surface-sensitive in-plane scattering at (1,0,0.1) from Cl and Br covered Cu(100) surfaces as a function of their potential. The different changes in the intensities for the (1,0,0.1) reflection with decreasing potential reveal an unlike structural behavior for the two halide species. Cycling of the potential within the known stability range of each p-(1×1) halide phase shows deviations of the intensity in the range of 10% at the upper limits of the potential window, respectively. The starting points of the potential cycles are marked by an arrow for Br and Cl covered Cu(100). While for Br the (1,0,0.1) intensity clearly decreases by 20% with a potential drop of 300 mV, the Cl-covered Cu(100) surface exhibits a plateau between $E_{\text{work}}=50$ mV and $E_{\text{work}}=-50$ mV and shows only slightly lower intensities at both borders of the plateau. This means that Br reacts more strongly and in a different manner on potential changes which is intuitively expected because of its larger polarizability in comparison to the more electronegative Cl. Fitting of all potential-dependent (1,0,0.1) reflection profiles leads to a constant peak position and full width at half maximum (Fig. 6). The fitted width of the in-plane reflections indicates an average domain size of 1050 Å. Out-of-plane reflections with $Q_z=0.5$, 0.97, and 1.94 that were scanned together with the in-plane data corresponding to Fig. 6 also showed no obvious or systematic peak broadening. The potential-induced change in the intensity implies, therefore, that besides the changes in the adlayer spacings or a decrease in its coverage no additional disorder or morphological roughening is induced.

The trend of little change in the surface-sensitive scattering signal of Cl on Cu(100) over the potential range from $E_{work}=-250$ mV to $E_{work}=+150$ mV is quantitatively expressed in the fact that neither the interlayer spacing of Cl-Cu nor that of the first two Cu layers shows any significant potential dependence. Both layer distances show constant elevated values in comparison to their bulk analog. Huemann *et al.*[21] found an expansion of the Cl-Cu distance of 5.8% and an expansion of 2.2% for the first Cu interlayer spacing. This means that we observe a potential-dependent crossover of the layer spacings induced by Br and Cl adsorption. At potentials below $E_{work}=-50$ mV the topmost Cu interlayer spacing are larger when the more polarizable Br is adsorbed on Cu(100). For potentials above $E_{work}=-50$ mV Cl leads to a larger separation of the topmost Cu layers.[21] This different influence on the bond-length expansion of the topmost Cu layer seems to be reflected by the fact that Cl containing solutions strongly facilitate the surface mobility of Cu under electrochemical conditions, while Br seems to inhibit such a Cu transport at the electrode surface for potentials above $E_{work}=-50$ mV.

This behavior of electrodeposited Cl on Cu(100) is rather different from that of dissociatively adsorbed Cl_2 molecules under UHV conditions despite the fact that Cl forms a $p(1\times1)$ adlayer structure in both cases. While the Cu-Cu layer distance at the surface is found to be at bulk value or slightly larger in UHV the Cl-Cu layer distance is up to 20% smaller than that found in this study.[42–45] The large difference in the Cl-Cu distance points toward an unlike electronic and binding state of the adsorbed Cl species which is obviously imposed by the different interfacial conditions at the Cu(100) surface.

A reasonable interpretation of the x-ray data presented here assumes *negatively charged* Cl anions that keep their charge upon adsorption on copper from an electrolyte and remain therefore largely *anionic*. The situation is different for the dissociative adsorption of *neutral* Cl_2 species under UHV conditions. Here we expect a partial charge transfer from the metallic substrate to the neutral adsorbate upon adsorption which could be understood in terms of an (partial) oxidation of the copper substrate. At the Cu/Cl/vacuum interface Cl species form relatively strong and therefore short bonds to the underlying copper substrate, while we find weaker and therefore more expanded Cu-Cl bonds at the respective Cu/Cl/electrolyte interface pointing to a more ionic character of these Cu-Cl bonds in the electrochemical environment. The net charge transfer from the Cl anion to the metal surface is low. The ionicity of Cl under electrochemical conditions can in part be understood as a result of the formation of a charged outer Helmholtz layer that forms above the inner Helmholtz layer constituted by the specifically adsorbed halide on the copper electrode. In this case dipoles of the water molecules and other cations accumulate in vicinity of the inner Helmholtz layer and thereby maintain the ionic state of the halide. In this respect one can regard the outer Helmholtz layer as a huge solvation shell of the inner Helmholtz layer. Such a solvation effect seems to have an impact also on the surface relaxation inside the electrode and explains the interlayer separations which are significantly higher in the electrochemical environment than under UHV conditions. In this simple picture it is not only the electronegativity which is higher for chlorine (3.16 according to the Pauling scale) than for bromine (2.96 according to the Pauling scale) that prevents adsorbed Cl from a potential-induced discharge in the electrochemical environment but it is also such a solvation effect. Br in the bulk solution and the adsorbed state shows a less pronounced tendency toward solvation. Hence, the interlayer spacings are more affected by potential effects.

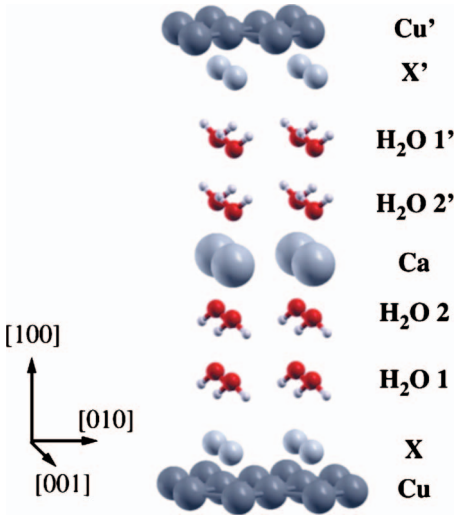

FIG. 7. (Color) Side view of the model for the simulation of the Helmholtz layer.

C. Quantum-chemical simulations

In order to support the above interpretation we also modeled the bonding of halide species at the Cu surface by DFT calculations for different electrochemical potentials at the copper electrode. Changes in the electrode potential were introduced by varying the total charge within the unit cell (which exhibits a linear relation with the Fermi energy). The solvent is taken into account by explicit inclusion of a small number of water molecules in the unit cell (Fig. 7). Electroneutrality of the electrolyte itself is guaranteed by adding the appropriate number of counterions to the unit cell. Due to the different reference states in the theoretical model and electrochemical experiments, no direct relation between calculated Fermi level and applied electrochemical potential is possible. We rather relate the change in the Fermi level with respect to the charge neutral cell to potential differences in the experiments, assuming a constant reference level in our calculations. In the following we present details of the computational setup.

The DFT calculations were performed with the exchange-correlation functional of Perdew and Wang[46] as implemented in the Vienna *ab initio* simulation program (VASP) (Refs. 47–49) using the projector augmented wave method to account for core electrons.[50,51] Within this approach surfaces are simulated by two-dimensional arrangements of atoms with a finite number of layers (slabs) that are periodically repeated in the direction of the surface normal but separated by a vacuum region which in our case is about 20.5 Å.

TABLE II. Calculated Br-Cu and first Cu-Cu layer spacings $d_{ad\text{-}1}$ and $d_{1\text{-}2}$ in units of the calculated Cu-Cu bulk spacing ($a/2$ =1.817 Å) as a function of the slab charge q_{slab}.

q_{slab} [$\lvert q_e \rvert$]	$d_{ad\text{-}1}$ [$a/2$]	$d_{1\text{-}2}$ [$a/2$]
0.25	1.056	1.000
0.00	1.077	1.003
−0.25	1.101	1.008

In preliminary test calculations we confirmed earlier results of Migani and Illas[30] for the copper bulk and the adsorption of Cl at Cu(100) in UHV in a $p(1\times1)$ adlayer structure for a coverage of $\theta=1$. In addition to the fourfold hollow position (Fig. 4) we have investigated the bridged and on-top positions for the adsorption of Cl and Br at Cu(100). The hollow position is more stable than the other two in agreement with experiment. We find a Br-Cu layer spacing of 1.83 Å and a Cl-Cu layer spacing of 1.67 Å for the UHV case. These values are 0.8% larger and −8.1% smaller than the optimized Cu-Cu bulk layer spacing of 1.817 Å, corresponding to $d_{ad\text{-}1}=1.008$ and 0.992, respectively. The first Cu-Cu layer spacing $d_{1\text{-}2}$ is increased by 0.3% (Br) and 0.6% (Cl) compared with the bulk value.

For a simulation of the electrochemical conditions the influence of an external potential and of the outer Helmholtz layer on the adsorption geometry was investigated. In order to model a negative (positive) potential we have added (subtracted) electrons to (from) the system as proposed by Taylor *et al.*[52] using charges of $q=-0.25|q_e|$, $q=0.00|q_e|$, and $q=0.25|q_e|$. This range approximately corresponds to the experimental potential window as can be concluded from the behavior of the Br-Cu layer distance $d_{ad\text{-}1}$ (see below). The resulting charge of the supercell (in the following denoted by the term slab charge q_{slab}) was compensated by a uniform background charge equal in magnitude but of opposite sign. As measure for the change in the electrochemical potential we calculated the change in the Fermi energy ΔE_{Fermi} for $q=-0.25|q_e|$ and $q=0.25|q_e|$ with respect to the neutral system. Here, an increase in the Fermi energy corresponds to a more negative potential. In order to simulate the outer Helmholtz layer, four layers of water molecules were added in the vacuum region and a layer of Ca counterions was placed in the central plane between the slabs to simulate the effect of the K^+ ions in a K*X* solution (Fig. 7). Ca^{2+} was used instead of K^+ in order to avoid too small distances between the ions in the central plane.

Although the chosen orientation of the water molecules is arbitrary we use this model as a first approximation to see the solvent effects on the adlayer structure. We carried out a full geometry optimization including the *a* vector perpendicular to the surface. The obtained results for the Br-Cu and first Cu-Cu layer spacings $d_{ad\text{-}1}$ and $d_{1\text{-}2}$ in units of the calculated Cu-Cu bulk layer spacing are shown in Table II for the different slab charges q_{slab}. The main effect of the outer Helmholtz layer is an outward movement of the Br atom as can be seen by comparing $d_{ad\text{-}1}=1.077$ for $q_{slab}=0.00|q_e|$ in Table II with $d_{ad\text{-}1}=1.008$ from the UHV calculations. Hydrogen bonds are formed between the Br atoms and the nearest water molecules. As a consequence, the Br-Cu bond is weakened. The experimental trend that the Br-Cu and the Cu-Cu layer spacings decrease monotonically with increasing potential i.e., with a decreasing ΔE_{Fermi} in our model, is clearly reproduced by the results of our simulations. The absolute calculated values of $d_{ad\text{-}1}$ (1.101, 1.077, and 1.056) agree well with the experiment, while the corresponding calculated changes in $d_{1\text{-}2}$ are smaller. In the case of Cl, the theoretical model calculations do not reproduce the experimental trend of $d_{ad\text{-}1}$. While the measured Cl-Cu distance is almost independent from the electrochemical potential, we find a similar trend as for Br.

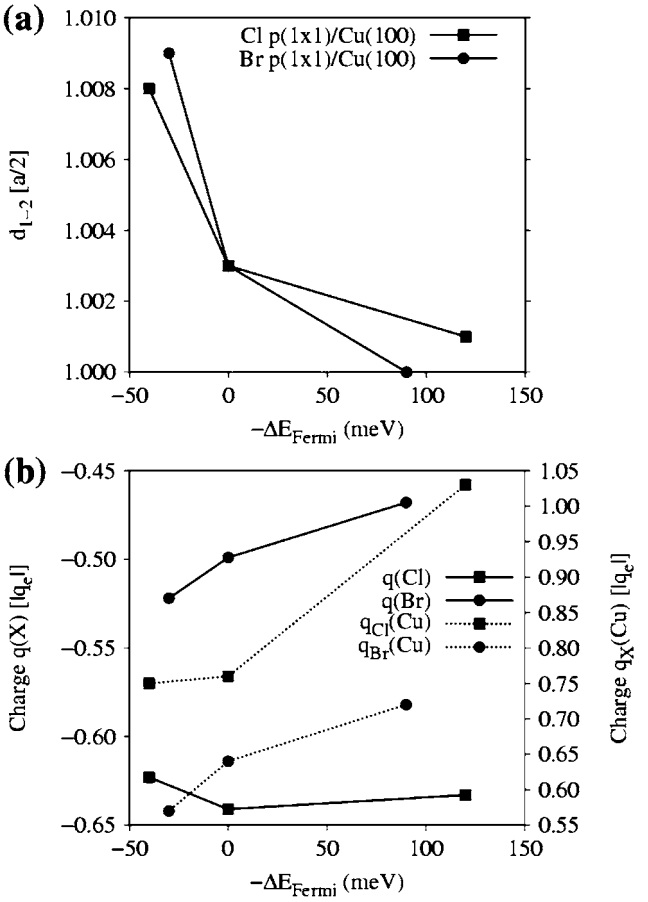

FIG. 8. (a) Change in the surface Cu-Cu layer spacing with the potential for the Cl and Br adsorptions, (b) atomic net charges $q(x)$ from a Bader analysis for X=Cl and X=Br (solid lines) and for the copper-slabs q_X(Cu) for X=Cl and X=Br (dashed lines).

Figure 8(a) shows a comparison of the potential-induced change in $d_{1\text{-}2}$ for Br and Cl adsorption. At high potential $d_{1\text{-}2}$, is larger with Cl than with Br. This difference decreases with decreasing potential and finally a crossing of the distances is observed, leading to a larger Cu-Cu layer spacing for the Br adsorption at more negative potential in agreement with the experimental trend. In the optimized structures of both adsorbates, the second Cu layer shows a very small buckling, in qualitative agreement with the experimental observations presented above. However, the differences in the Cu *z* coordinates are within the numerical errors of the optimization procedure and will therefore not be discussed.

Finally, we have performed a Bader analysis[53–55] in order to investigate the change in the charge $q(X)$ and the total charge of the copper slab $q_x(\mathrm{Cu})$ for $X=\mathrm{Cl}$ and $X=\mathrm{Br}$ in dependence of the potential [Fig. 8(b)]. The adsorbed Cl is always more negative than Br as can be expected from the difference in electronegativity of both species. But while the negative charge of the adsorbed Br decreases with increasing potential, the charge of the adsorbed Cl is almost constant. Furthermore, the charge of the copper slab $q_{\mathrm{Cl}}(\mathrm{Cu})$ increases much stronger than $q_{\mathrm{Br}}(\mathrm{Cu})$ with increasing potential. This can be explained by a larger polarizability of adsorbed Br and consequently a larger charge transfer from Br to the copper than in the case of Cl already for a constant coverage.

IV. CONCLUSIONS

Electrochemically adsorbed bromide forms a $p(1\times1)$ adlayer geometry on Cu(100) with reference to a conventional choice of the substrate unit cell. The most important result of this *in situ* x-ray study is the quantitative analysis of the adlayer induced and potential-dependent relaxation of the Cu(100) electrode surface. The Br-Cu spacing and the topmost Cu-Cu layer distances are significantly expanded by 8.3% and by 3.2% compared to the CuBr and Cu bulk value at $E_{\mathrm{work}}=-150$ mV, respectively. As the potential is increased to $E_{\mathrm{work}}=+50$ mV these spacings decrease continuously by 4.1% and 2.1% in the potential range of $E_{\mathrm{work}}=-150$ mV to $E_{\mathrm{work}}=+50$ mV. Both layer spacings remain expanded at $E_{\mathrm{work}}=+50$ mV with reference to their bulk analog. The topmost Cu-Cu spacing is also still expanded by 1.1% at $E_{\mathrm{work}}=+50$ mV. The second Cu layer experiences a potential-dependent buckling due to the different second-shell coordination geometry of Cu by bromide. The potential-dependent behavior of the Br-Cu interface points toward a charge transfer into the Cu substrate with increasing potential and a strengthening of the Cu-Cu bond at the electrode surface. As a result the Cu mobility is notably reduced (at positive potentials) at the electrode surface in comparison to Cl containing electrolytes.

First-principles quantum-chemical calculations confirm the experimentally observed trends of the Br-Cu and Cu-Cu spacing expansions with decreasing potential. If the total charge is changed in order to vary the Fermi energy of the metal surface, also the atomic charge of the Br atoms changes. The Br-Cu spacing is decreasing with increasing negative charge. A crossing of the Cu-Cu layer spacing $d_{1\text{-}2,\mathrm{Cl}}$ and $d_{1\text{-}2,\mathrm{Br}}$ with decreasing potential was found. The theoretical calculations show that interaction of Br and Cl with solvent molecules plays an important role for the interlayer spacings. The Br-Cu spacing in the presence of water is significantly increased compared to ultrahigh vacuum conditions. There is still a discrepancy between the measured and calculated potential dependences of the Cl-Cu spacing. The theoretical models predict a similar trend as for the Br-Cu spacing. A possible reason is that the range of cell charges introduced in the theoretical models does not correspond to the experimental potential window. On the other hand, the agreement between calculated and measured Br-Cu spacings is almost quantitative. It is therefore more likely that other reasons, the neglect of anion-specific solvation effects and potential-dependent coverage changes in our models, are more relevant. These effects will be addressed in future studies.

ACKNOWLEDGMENTS

We greatly appreciate the help of our colleague Peter Königshofen who built the electrochemical cell and made important contributions to its functionality.

*Corresponding author: peter.broekmann@iac.unibe.ch

[1] P. C. Andricacos, C. Uzoh, J. O. Dukovic, J. Horkans, and H. Deligianni, IBM J. Res. Dev. **42**, 567 (1998).
[2] T. P. Moffat, D. Wheeler, and D. Josell, Abstr. Pap. - Am. Chem. Soc. **230**, U1157 (2005).
[3] T. P. Moffat, D. Wheeler, and D. Josell, J. Electrochem. Soc. **151**, C262 (2004).
[4] T. P. Moffat, D. Wheeler, W. H. Huber, and D. Josell, Electrochem. Solid-State Lett. **4**, L5 (2001).
[5] D. Josell, D. Wheeler, W. H. Huber, J. E. Bonevich, and T. P. Moffat, J. Electrochem. Soc. **148**, C767 (2001).
[6] K. Doblhofer, S. Wasle, D. M. Soares, K. G. Weil, G. Weinberg, and G. Ertl, Z. Phys. Chem. **217**, 479 (2003).
[7] K. Doblhofer, S. Wasle, D. M. Soares, K. G. Weil, and G. Ertl, J. Electrochem. Soc. **150**, C657 (2003).
[8] D. W. Suggs and A. J. Bard, J. Phys. Chem. **99**, 8349 (1995).
[9] O. M. Magnussen, M. R. Vogt, J. Scherer, A. Lachenwitzer, and R. J. Behm, Mater. Corros. **49**, 169 (1998).
[10] M. R. Vogt, A. Lachenwitzer, O. M. Magnussen, and R. J. Behm, Surf. Sci. **399**, 49 (1998).
[11] O. M. Magnussen and M. R. Vogt, Phys. Rev. Lett. **85**, 357 (2000).
[12] O. M. Magnussen, L. Zitzler, B. Gleich, M. R. Vogt, and R. J. Behm, Electrochim. Acta **46**, 3725 (2001).
[13] O. M. Magnussen, Chem. Rev. **102**, 679 (2002).
[14] O. M. Magnussen, J. Hageböck, J. Hotlos, and R. J. Behm, Faraday Discuss. **94**, 329 (1992).
[15] P. Broekmann, M. Wilms, M. Kruft, C. Stuhlmann, and K. Wandelt, J. Electroanal. Chem. **467**, 307 (1999).
[16] D. Wang, R. D. Mikkola, C. Wu, and G. G. Barclay, U. S. Patent Publication Application, Pub. No. 2006/0016693 A1 (2006).
[17] C. Safarowsky, K. Wandelt, and P. Broekmann, Langmuir **20**, 8261 (2004).
[18] D.-T. Pham, K. Gentz, C. Zörlein, N. T. M. Hai, S.-L. Tsay, B. Kirchner, S. Kossmann, K. Wandelt, and P. Broekmann, New J. Chem. **30**, 1439 (2006).
[19] D.-T. Pham, S.-L. Tsay, K. Gentz, C. Zoerlein, S. Kossmann, J.-S. Tsay, B. Kirchner, K. Wandelt, and P. Broekmann, J. Phys. Chem. C **111**, 16428 (2007).
[20] P. Broekmann, W. Lisowski, M. Anastasescu, A. Speanig, and K. Wandelt, J. Electroanal. Chem. **500**, 241 (2001).
[21] S. Huemann, N. T. M. Hai, P. Broekmann, K. Wandelt, H.

Zajonz, H. Dosch, and F. Renner, J. Phys. Chem. B **110**, 24955 (2006).
[22] R. Dronskowski, *Computational Chemistry of Solid State Materials* (Wiley-VCH, Weinheim, 2005).
[23] L. G. M. Pettersson and P. S. Bagus, Phys. Rev. Lett. **56**, 500 (1986).
[24] K. Doll and N. M. Harrison, Chem. Phys. Lett. **317**, 282 (2000).
[25] A. Migani, C. Sousa, and F. Illas, Surf. Sci. **574**, 297 (2005).
[26] A. Migani and F. Illas, J. Phys. Chem. B **110**, 11894 (2006).
[27] P. S. Bagus, D. Käfer, G. Witte, and C. Woll, Phys. Rev. Lett. **100**, 126101 (2008).
[28] S. Venkatachalam, P. Kaghazchi, L. A. Kibler, D. M. Kolb, and T. Jacob, Chem. Phys. Lett. **455**, 47 (2008).
[29] E. Schreiner, N. N. Nair, and D. Marx, J. Am. Chem. Soc. **130**, 2768 (2008).
[30] A. Migani, C. Sousa, F. Sanz, and F. Illas, Phys. Chem. Chem. Phys. **7**, 3353 (2005).
[31] C. D. Taylor, S. A. Wasileski, J. S. Filhol, and M. Neurock, Phys. Rev. B **73**, 165402 (2006).
[32] C. D. Taylor, R. G. Kelly, and M. Neurock, J. Electroanal. Chem. **607**, 167 (2007).
[33] D. M. Kolb, Ber. Bunsenges. Phys. Chem. **98**, 1421 (1994).
[34] M. Wilms, M. Kruft, G. Bermes, and K. Wandelt, Rev. Sci. Instrum. **70**, 3641 (1999).
[35] P. Broekmann, N. T. M. Hai, and K. Wandelt, J. Appl. Electrochem. **36**, 1241 (2006).
[36] N. T. M. Hai, B. Gasparovic, K. Wandelt, and P. Broekmann, Surf. Sci. **601**, 2597 (2007).
[37] I. K. Robinson, Phys. Rev. B **33**, 3830 (1986).
[38] S. Hull and D. A. Keen, Phys. Rev. B **50**, 5868 (1994).
[39] W. Bührer and W. Haelg, Electrochim. Acta **22**, 701 (1977).
[40] I. M. Tidswell, N. M. Markovic, and P. N. Ross, Phys. Rev. Lett. **71**, 1601 (1993).
[41] I. M. Tidswell, N. M. Markovic, and P. N. Ross, J. Electroanal. Chem. **376**, 119 (1994).
[42] L. Q. Wang, A. E. Schach von Wittenau, Z. G. Ji, L. S. Wang, Z. Q. Huang, and D. A. Shirley, Phys. Rev. B **44**, 1292 (1991).
[43] P. H. Citrin, D. R. Hamann, L. F. Mattheiss, and J. E. Rowe, Phys. Rev. Lett. **49**, 1712 (1982).
[44] F. Jona, D. Westphal, A. Goldman, and P. M. J. Marcus, J. Phys. C **16**, 3001 (1983).
[45] J. R. Patel, D. W. Berreman, F. Sette, P. H. Citrin, J. E. Rowe, P. L. Cowan, T. Jach, and B. Karlin, Phys. Rev. B **40**, 1330 (1989).
[46] Y. Wang and J. P. Perdew, Phys. Rev. B **44**, 13298 (1991).
[47] G. Kresse and J. Hafner, Phys. Rev. B **49**, 14251 (1994).
[48] G. Kresse and J. Furthmüller, Comput. Mater. Sci. **6**, 15 (1996).
[49] G. Kresse and J. Furthmüller, Phys. Rev. B **54**, 11169 (1996).
[50] G. Kresse and D. Joubert, Phys. Rev. B **59**, 1758 (1999).
[51] P. E. Blöchl, Phys. Rev. B **50**, 17953 (1994).
[52] C. D. Taylor, S. A. Wasileski, J.-S. Filhol, and M. Neurock, Phys. Rev. B **73**, 165402 (2006).
[53] R. Bader, *Atoms in Molecules: A Quantum Theory* (Oxford University Press, New York, 1990).
[54] G. Henkelman, A. Arnaldsson, and H. Jónsson, Comput. Mater. Sci. **36**, 354 (2006).
[55] E. Sanville, S. D. Kenny, R. Smith, and G. Henkelman, J. Comput. Chem. **28**, 899 (2007).